CFD analysis of hydrogen injection pressure and valve profile law effects on backfire and pre-ignition phenomena in hydrogen-diesel dual fuel engine

A. Menaa, M.S. Lounici, F. Amrouche, Khaled Loubar, M. Kessal

CFD Analysis of Hydrogen Injection Pressure and Valve Profile Law Effects on Backfire and Pre-ignition Phenomena in Hydrogen-Diesel Dual Fuel Engine

A.Menaa[1, 2], M.S. Lounici[3], F. Amrouche[1], K.Loubar[4], M. Kessal[2]

[1*]Centre de Développement des Energies Renouvelables, Route de l'Observatoire BP. 62 Bouzaréah 16340 Alger, Algérie.

[2]Laboratoire de Génie Physique des Hydrocarbures, Faculté des Hydrocarbures et de la Chimie, Université M'Hamed BOUGARA Boumerdès 3500 Algérie.

[3]Laboratoire d'énergétique, mécanique et ingénieries, UMBB, Boumerdès, 35000, Algérie.

[4]GEPEA, UMR6144, Département Systèmes Energétique et Environnement, Ecole des Mines de Nantes .4 rue Alfred Kastler, BP20722, 44307, Nantes, France

Abstract

This paper focuses on optimizing the hydrogen TMI (timed manifold injection) system through valve lift law and hydrogen injection parameters (pressure, injection inclination and timing) in order to prevent backfire phenomena and improve the volumetric efficiency and mixture formation quality of a dual fuel diesel engine operating at high load and high hydrogen energy share. This was achieved through a numerical simulation using CFD code ANSYS Fluent, developed for a single cylinder hydrogen-diesel dual

fuel engine, at constant engine speed of 1500 rpm, 90% of load and 42.5% hydrogen energy share. The developed tool was validated using experimental data. As a results, the operating conditions of maximum valve lift=10.60 mm and inlet valve closing=30 °CA ABDC (MVL10 IVC30) prevent the engine from backfire and pre-ignition, and ensure a high volumetric efficiency. Moreover, a hydrogen start of injection of 60 °CA ATDC (HSOI60) is appropriate to provide a pre-cooling effect and thus, reduce the pre-ignition sources and helps to quench any hot residual combustion products. While, the hydrogen injection pressure of 2.7 bar and an inclination of 60°, stimulate a better quality of hydrogen-air mixture. Afterwards, a comparison between combustion characteristics of the optimized hydrogen-diesel dual fuel mode and the baseline (diesel mode) was conducted. The result was, under dual fuel mode there is an increase in combustion characteristics and NOx emissions as well as a decrease in CO2 emissions. For further improvement of dual fuel mode, retarding diesel start of injection (DSOI) strategy was used.

Keywords: Hydrogen-diesel dual fuel mode; Hydrogen TMI system; Hydrogen injection parameters; valve lift law; CFD Analysis.

1. Introduction

Renewable hydrogen while used as fuel can help to overcome both fossil fuel depletion and air pollution [1]. Indeed, hydrogen has very attractive combustion properties such as high diffusivity, high flame speed and wide flammability range. These last are very helpful to improve energetic and environmental engine performances. However, abnormal combustion such as backfire [2,3], pre-ignition [4,5], and knock phenomenon [3,4] can occur while using hydrogen in internal combustion engine. The backfire or pre-ignition decreases the power output of an engine [1,6]. Moreover, the rise of the intake manifold pressure resulting from backfire and pre-ignition is susceptible to harm the intake system [7]. To prevent backfire, eliminating ignition source in contact with hydrogen-air mixture in the intake manifold can be used. In the literature, several solutions have been proposed to achieve this condition, such as (i) decreasing the overlap period, (ii) retarding the timing of the inlet valve opening (iii) using leaner mixtures, (iv) implementing exhaust gas recirculation and (v) intake air cooling systems [8-10]. On the other hand, pre-ignition phenomena produce an increased chemical heat release rate, that lead to a rapid pressure rise, acoustic oscillation and higher surface temperature. The later can further advance the start of combustion, which in turn leads to a runaway effect, and if left unchecked will lead to engine failure [11]. According to Verhelst et al. [7], the presence of pre-ignition in internal combustion engine causes the symmetrical phasing of the in-cylinder pressure, which leads to a drop of the indicated mean effective pressure

(IMEP) to almost zero. For hydrogen engines, pre-ignition is more pronounced when the hydrogen-air mixture is near the stoichiometric condition [7], and this limits the equivalence ratio for this kind of engines [11]. Pre-ignition is the result of various conditions such as an increase in the engine speed and load [7], an increase in the inlet pressure or inlet temperature and an increase in the compression ratio [11]. Numerous studies have been done to overcome pre-ignition in internal combustion engine and several strategies have been proposed to achieve this goal [9-12] among which, a use of an intake charge cooling system; a cold spark plugs and aged sodium filled valve [10] or the implementation of a variable valve timing strategy for effective scavenging of exhaust residual. The control of ignition advance and design of appropriate hydrogen induction system were also used to overcome pre-ignition [7,11]. Das et al. [12] designed a hydrogen timed manifold induction system that helps to pre-cool the charge, which leads to quench and dilute any residual combustion product that could be present in the compression space near top deed center (TDC). Thus, hydrogen induction methods can play a critical role in the development of a practical hydrogen engine [12]. In fact, with a specific design, hydrogen induction system can prevent abnormal combustion such as backfire and pre-ignition [10] and can also allow an ultra-lean combustion regime to be achieved with high volumetric efficiency, high thermal efficiency and lower NOx emissions [10]. In practical, there are five techniques to introduce hydrogen in internal combustion engines; Carburation, Continuous Manifold Injection (CMI), Timed

Manifold Injection (TMI), Low Pressure Direct Injection (LPDI) and High Pressure Direct Injection (HPDI) [1,10,12]. The first method is the simplest technique because it does not require a major modification in the existing engine [10] and ensures a homogeneous hydrogen-air mixture [4]. However, the carburation increases the risk of backfire in hydrogen internal combustion engine [10] and reduced volumetric efficiency and power outlet of the engine since the gas replaces some amount of intake air [4]. The same problems are encountered in CMI. However using hydrogen direct injection prevents pre-ignition and backfire [1,12] and induce higher volumetric efficiency compared to other techniques [13]. But it requires an injector that could resist to higher combustion temperature and prevent corrosion. Furthermore, a specific design of the injector is necessary to ensure a better lubrication between the injector moving parts [1]. Another problem with direct injection is that the time allowed for mixing of hydrogen and air after injection is very short [12] and this affects the combustion efficiency.

The fourth technique which is TMI is the most efficient technique to introduce the hydrogen in the internal combustion engine. Indeed, an appropriately designed TMI system can eliminate undesirable combustion phenomena such as backfire and pre-ignition, increase engine performance and decrease pollutants emission levels [1,5,12,14]. Moreover, this technique does not require any radical modifications in the existing system [14], and it has the capacity to start fuel delivery at a timing position sometimes after the beginning of intake stroke [5]. Consequently, the TMI embodies the advantages

of direct injection technique and carburetor one i.e. it eliminates both pre-ignition and backfire phenomena and ensures a homogenous hydrogen air mixture in the combustion chamber.

For engines implemented with TMI system, hydrogen injection parameters such as the injection pressure and timing, injection position, injection nozzle area (diameter), and injector inclination, have a significant effect on combustion performance, emissions and abnormal combustion [15,16]. Through the literature, different studies have been performed to identify the effect of these parameters on engine performances. Wang et al. [16] have established a 3D simulation model for a port fuel injection hydrogen internal combustion engine using AVL Fire software to investigate the quality of the hydrogen air mixture formation and the combustion characteristics of the hydrogen fueled engine under different hydrogen injection timings, nozzle hole positions and nozzle hole diameter. According to their results, an optimum choice of the hydrogen injection parameters is required to improve the uniformity of the hydrogen-air mixing in the cylinder and the combustion characteristics. Chintala et al. [17] have used a CFD software to investigate the effect of the gas injector angle and location on gas (CNG or H_2) - air mixture formation, backfiring and thermal efficiency at different injection pressure and engine speed. They observed that the mixture velocity and engine speed are the key parameters for the optimization of the critical distance of the gas injector between the injector mounting point and inlet valve axis in intake manifold of a dual-fuel engine.

According to their results, the critical distance decreases with increasing engine speed at a constant injection pressure while it increases with increasing injection pressure at a constant engine speed. They also conclude that the gas injector for CNG and H_2 fuel needs to be mounted on intake manifold within the critical distance in order to avoid fuel accumulation and backfiring. In addition, they observed that mixing rate of gaseous fuel with air increases with increasing gas injection pressure. On the other hand, Liu et al. [6] numerically investigated the effect of injection timing on hydrogen-air mixture formation at different engine speeds and equivalence ratio of a hydrogen internal combustion engine. They conclude that the backfire event is mainly related to the concentration of hydrogen residual at the intake ports in the manifold injection, thus, the leaner the concentration of the residual, the lower possibility of the backfire event. Moreover, according to this research, a limited injection end timing is required to prevent backfiring risk. Cheng et al. [18] evaluated the effect of hydrogen injection timing on mixture formation, power output, thermal efficiency, cycle-to-cycle variation and backfiring at different engine speeds and loads. They could evaluate an optimized hydrogen injection timing for various engine speeds and loads. Yang et al. [19] studied the effect of natural gas injection timing on the performance and emission of a turbocharged dual fuel common rail engine under different pilot injection timing and pressure at low load. They reported that retarded natural gas injection timing could achieve a stratified-like air–fuel mixture in the cylinder under different pilot injection conditions. This provided a method

138 to improve combustion performance and exhaust emissions at low loads. Saravanan et al.
139 [20] experimentally studied the effects of the hydrogen injection timing and duration on
140 performance and emissions of a DI diesel engine at various loads. They could define
141 optimum operating conditions for which an increased thermal efficiency and reduced
142 azote oxide (NOx), carbon monoxide (CO), carbon dioxide (CO_2) and unburned
143 hydrocarbon (HC) emissions were observed. Yang et al. [21] numerically investigated the
144 effects of three hydrogen injection modes and nozzle diameter on mixture formation and
145 combustion performance at different equivalence ratio and engine speed in a hydrogen
146 fueled spark ignition engine with port fuel injection. They found that using spaced dual
147 injection improves hydrogen-air mixture uniformity and combustion velocity, increases
148 NOx emission and reduces the probability of backfire. They also reported that the
149 uniformity coefficient decreases gradually and the indicated power and indicated thermal
150 efficiency increased first and then decreased with increasing the nozzle diameter.
151 Chintala et al. [22] numerically investigated the effect of water injection on the maximum
152 hydrogen share limited by mixture auto-ignition and knocking problem in hydrogen
153 based dual fuel engine. They observed that it could be increased from 18.8% with
154 conventional dual fuel engine to 60.7% with water injection at 100% full load. Salvi et al.
155 [23] experimentally studied the effect of volumetric compression ratio, spark timing and
156 exhaust gas recirculation (EGR) on engine performance, emission characteristics and
157 backfire occurrence in a hydrogen fuelled spark ignition engine. They found that with an

optimum choice of compression ratio, EGR and spark timing, the thermal efficiency and NOx emission are improved and the risk of backfire occurrence is reduced. Tsujimura et al. [24] modified a diesel engine to work on direct injection hydrogen engine with EGR and supercharging. They experimentally studied the effect of various operating parameters such as: hydrogen injection timing, pressure injection, spark ignition timing, intake oxygen concentration and equivalence ratio, on NOx emission and thermal efficiency. Moreover, they studied the effect of intake and exhaust valve closing timing. They found a significant decrease of NOx emission (100 ppm) and increase of indicated thermal efficiency (+50%) for optimal values of the previous operating parameters. Dhyani et al. [25] experimentally analyzed the effect of knocking on backfire in a multi-cylinder hydrogen engine. They investigated its control by varying spark timing and hydrogen injection timing. They found that knocking combustion can be linked with backfire, as probability of backfire occurrence decreases with the reduction in knocking risk. In addition, they reported that retarded spark timing and delayed hydrogen injection timing reduce the risk of backfire occurrence. Dhyani et al. examined, in another experimental study [26], the effect of cooled EGR and water injection strategies on the possibility of backfire occurrence, NOx emission and performance of a multi-cylinder hydrogen engine. They found a reduction of backfire occurrence probability and NOx emissions using both strategies without affecting brake thermal efficiency. They also

reported that water injection strategy is more efficient as compared to cooled EGR to control backfire occurrence with ultra-low (near zero) NOx emission.

Other parameters, like valve lift law, inlet valve close (IVC) timing, inlet valve open (IVO) timing and maximum valve lift, may also have a great importance in the control of abnormal combustion, volumetric efficiency, engine performance and exhaust emissions of an engine equipped with TMI system. Some researchers focused on these parameters to improve engine efficiency. Jia et al. [27] numerically investigated the effect of IVC timing and Start of Injection (SOI) on combustion performance and emissions of a diesel premixed charge compression ignition (PCCI) engine. They found out that IVC timing and SOI affect the ignition timing, combustion temperature and effective compression ratio. They concluded that adjusting IVC and SOI can optimize engine emissions, fuel economy and ringing intensity. Moreover, Zhang et al. [28] experimentally evaluated the influence of the late inlet valve closing (LIVC) and the rebreathing valve strategies of inlet and exhaust valve (second opening of inlet/exhaust valves) on combustion characteristics and exhaust emissions of a diesel engine at low loads. They have suggested using the rebreathing valve strategies at lower engine loads, and the standard and late IVC strategies at higher loads to improve emission and combustion characteristics. Xu et al. [29] used an electromagnetic inlet valve train (EMIV) to regulate the inlet valve control parameters in order to improve the performance of a gasoline engine. They could analyze the influence of inlet valve train on the intake charging,

power consumption and pumping loss of a gasoline engine. They found out that with an optimized valve law, the intake charging can be improved and power consumption reduced, therefore they conclude that the application of EMIV is an effective system to improve the performance of the engine. Li et al. [30] numerically investigated the influence of intake backflow on the in-cylinder situation and auto ignition of a gasoline engine. They observed a decrease of the mean temperature with increasing the intake backflow. Moreover, they found out that the auto ignition timing first delayed, then, advanced as the intake backflow increased. Çinar et al. [31] experimentally studied the impact of the valve lift on in-cylinder pressure, heat release rate, engine performance and exhaust emissions of a Homogeneous Charge Compression Ignition (HCCI) gasoline engine. They observed an improvement in engine performance, reduction in exhaust emissions with extended range of engine operation without knock when using a low valve lift. Finally, Verhelst et al. [32] while investigating the impact of variable valve timing on power, emissions and backfire of a bi-fuel hydrogen/gasoline engine, found that variable valve timing is a way to improve power output, reduce NOx emission and avoid backfiring risk.

Through the literature, it can be seen that few researches focus simultaneously on the effect of injection parameters and valve lift law on backfiring, intake charging and mixture formation of a dual fuel hydrogen-diesel engine. Therefore, there is a crucial need to conduct the related study. The aim of this work is to optimize a hydrogen TMI

system through valve lift law (maximum valve lift and IVC timing) and hydrogen injection parameters (pressure, inclination and injection timing) in order to prevent backfire phenomena, improve volumetric efficiency and mixture formation quality of a dual-fuel diesel engine. To achieve this goal, a numerical simulation using CFD code ANSYS Fluent was developed and validated with experimental data.

2. Numerical approach

2. 1. Geometric configuration and mesh generation

The engine simulated is a Lister Petter TS1 mono cylinder, four strokes direct injection diesel engine with a displacement of 0.63 liters. The engine and diesel fuel injector characteristics are given in Table 1. For dual fuel mode, hydrogen is injected in the intake manifold. The inlet and exhaust duct geometry with gas injector position is shown in Fig. 1. The distance between the hydrogen injector and intake valve (P_0 - P_1) is set to 150 (mm), the hydrogen injector prototype chosen for this study is DYMCO Corp/GISM-i1000, the characteristics of the injector are summarized in Table 2.

Because the number of cases to investigate is significant, the 3D simulation requires an excessive calculation time. For this reason, 2D approach has been first adopted to the choice of intake valve law (MVL and IVC). Then, the results of this approach have been

compared to 3D ones and validated using experimental data [33]. Afterwards, 3D simulation approach was used to select the hydrogen injector parameters (hydrogen start of injection, hydrogen injection pressure and hydrogen injector inclination). Finally, these results were used for the full cycle simulation.

For 2D and 3D geometry, the computational domain was divided into sub-volume (multi-block methods). In 2D geometry, the structured mesh is used with a quadrilaterals cell shape for the totally sub-volume. In 3D geometry, the structured mesh is used with a hexahedral cell shape for all sub-volume except for the intake port, exhaust port and the contact region between injector and intake manifold that have an unstructured mesh with a tetrahedral cell shape as it is shown in Fig. 2.

The main challenge to simulate a three-dimensional internal combustion engine is the dynamic mesh due to moving boundaries such as cylinder, valves and piston head [34]. Three methods exist to update the mesh of a moving boundary project: smoothing, re-meshing and layering [35]. In our case the layering method has been adopted, Fig. 2 shows the engine mesh at TDC and BDC. The intake and exhaust valve dynamic mesh is assumed by a valve profile using a user defined function (UDF). Fig. 3 shows the valve lifts profiles for various IVC and MVL; the law of valve lift is given by following equation [33]:

$$l_v = \frac{\text{MVL}}{2}\left[1 - cos\left(\frac{2\pi\theta + C + AO}{AO + RC + 180}\right)\right]$$

MVL **:** Maximum Valve Lift (mm)

θ: Crank Angle Degree (°CA)

AO: Advance Opening (°CA)

RC: Retard Closing (°CA)

C: Constant (=180 (°CA) for exhaust and 360 (°CA) for intake).

2. 2. Numerical modeling procedure and validation

The CFD code used in this study is ANSYS Fluent v16.0. Pressure based solver and coupled scheme for pressure-velocity coupling were used. The second order implicit scheme was chosen for temporal discretization. For spatial discretization, the second order scheme was chosen for pressure and second order upwind for density, momentum and turbulent kinetic energy. In this work, the residual is set to 10^{-6}. The energy equation is solved for all cases to calculate the temperature evolution. In order to relate the pressure with temperature and density the state equation is also used, the charge (air, mixing gas) was assumed as ideal gas [21, 38]. The turbulent flow was modeled using the k-ε RNG model [40, 41]. The "discrete phase" model available in ANSYS Fluent makes it possible to simulate the two-phase jet in the combustion chamber. This model uses several sub-models that can define; droplet size, velocity distribution, sprays angle,

particle trajectory, spray breakup, collision, coalescence and particle evaporation. For breakup of the jet, the wave model of Reitz was used. This model considers that the breakup of the liquid jet is due to the relative velocity difference between the liquid phase and the gaseous phase, this model is the most popular used for high injection pressure [38,39]. The combustion model chosen for this study is laminar finite rate/eddy dissipation scheme [22,39,40], with one reaction for diesel and one reaction for hydrogen. The reaction rate is equal to the minimum of the laminar finite rate or eddy dissipation scheme. For the ignition delay, the Hardenberg & Hase (H&H) correlation is chosen [40, 42]. The ignition is ensured by the diesel fuel in dual fuel engine mode; therefore, the ignition delay correlation was applied to the diesel fuel. NOx considered in this study are thermal and prompt [36, 42]. The extended Zeldovich mechanism is used for thermal NOx formation and Fenimore mechanism for prompt NOx [36].

Boundary conditions chosen for this study are the atmospheric pressure for air inlet and gaseous mixture outlet, and a fixed temperature for inlet and outlet. The values are taken from experimental measurements. For hydrogen inlet boundary condition, mass flow rate type was selected and applied at the inlet area of the injector (fig. 2). For this, an UDF is developed to introduce the mass flow rate as a function of crank angle for each corresponding hydrogen injection pressure at a fixed energy share and engine speed, taking in consideration the opening and closing time and the injection duration.

The wall heat transfer losses are estimated by Hohenberg correlation. To introduce the empirical heat transfer correlation, a user defined function is developed and implemented successfully. The Hohenberg model performs best comparing with the others correlations [41]. Two full cycles were realized in a single simulation. Each simulation was initiated at Top Dead Center (TDC) during the intake stroke. For the first cycle, the hybrid initialization provided by ANSYS Fluent is used. In the second cycle, the initial values of the parameters are obtained from the results of the first cycle. This second cycle is the cycle considered in all our investigations.

2.3. Grid sensitivity study

Mesh generation is a critical step to build multi-dimensional CFD engine model because the mesh quality has a significant impact on the numerical stability of the CFD solver and the mesh density which can affect the simulation results [36]. Several grids were created and examined. Table 3 shows the number of cells at TDC and BDC.

Fig. 4 (a) shows the in-cylinder mass evolution under different mesh refinement. It can be seen that no significant difference was observed with mesh refinement. The maximum deviation is less than 0.25 % in the 2D approach and less than 0.06 % in the 3D simulation. Considering both computational time and the quality of results, case 7 is chosen for the 2D mesh and the case 5 for the 3D simulation (Table 3).

2.4. Time step sensitivity study

For the study of the time step sensitivity, the in-cylinder mass evolution is used in such a way that when the two valves are closed, the mass in the combustion chamber is constant. Fig. 4 (b) shows the evolution of in-cylinder mass for different crank angle step size in cases of 2D and 3D simulations. For the 2D simulation, 0.1 and 0.05 (°CA) verified mass conservation, therefore, the time step chosen is 0.05 (°CA). For 3D simulation 0.1 (° CA) time steps is chosen. These choices take in consideration simulation time.

2.5. Comparison between 2D and 3D simulations

For 2D approach, the geometry was modified in order to verify the volumetric compression ratio, a constant depth was introduced, the bowl was removed and the squish clearance was adjusted accordingly (see Fig.2).

Fig. 5 shows the in-cylinder volume and mass profiles with the 2D and 3D simulations. For the in-cylinder volume profiles, the two curves are almost similar. However, there is a slight difference during intake stroke that can be caused essentially by the depth value of valve. For the in-cylinder mass profiles, a small difference exists between the 2D and 3D simulations; this difference is probably due to the inlet valve reference flow area and discharge coefficient. The error in in-cylinder mass is less then 4.0 %. Therefore, it can be concluded that the 2D approach reproduces the 3D simulations.

2.6. 2D - 3D validation

Fig. 6 shows the comparison of in-cylinder pressure profiles of a cold flow between the experimental results [33] and 2D and 3D numerical results. The numerical and experimental results are in good agreement. However, a slight difference was noticed, and the error in the maximum pressure is 0.88 (bar) (1.68%) in 3D simulation and 1.75 (bar) (3.6%) in 2D simulation. The 2D and 3D simulations are therefore validated.

In this study, first, the intake valve lift law (MVL and IVC) is optimized using 2D approach. The results of the optimal intake valve lift law are then confirmed with a 3D simulation. Then, hydrogen injector parameters (HSOI, hydrogen injection pressure and injector inclination angle) are optimized with 3D simulation. Afterwards, the engine performance of both diesel and dual fuel modes are analyzed, and finally the diesel start of injection (DSOI) is optimized for dual fuel mode. The method of step by step is adopted to optimize each considered parameter. When the effect of one parameters on dual-fuel diesel engine operating mode is studied, the others parameters were kept at a fixed value, then, the fixed value is replaced by the optimal value for each investigated parameter successively.

3. Results and discussion

3. 1. Valve lift law

The selection of the valve lift law has been done by analyzing the in-cylinder mass, backflow mass, maximum pressure and aspiration work using a 2D approach for the cold airflow case. To achieve this goal, three maximum valve lift (MVL10.6, MVL8.0 and MVL6.0 mm) combined with three intake valve closing (IVC70, IVC50 and IVC30 °CA ABDC) for seven engine speeds (from 1000 to 2500 rpm), were examined. This represents 63 cases.

The in-cylinder mass is the value of mass evolution inside the cylinder after the intake valve close. Fig. 7 (a) shows the effect of MVL and IVC on the in-cylinder mass for different engine speeds. At early IVC (IVC30), the in-cylinder mass decreases with speed for all cases. While at IVC50, the variation of the in-cylinder mass still slightly decreasing with speed for MVL6.00 however, it was almost negligible for the other cases. At late IVC (IVC70), the in-cylinder mass increases lightly with the speed for all MVL investigated. These results can be explained by the fact that the time allowed to the airflow is more significant in late IVC at high speeds. Jiangtao Xu et al [29] indicated that the volumetric efficiency increases for early IVC at low speeds and decreases at high speeds. Therefore, for late IVC, the volumetric efficiency decreases at low speeds and increases at high speeds. Our results are in concordance with those finding.

For early IVC, the intake charge increases with the increase of MVL, especially at high speeds. On the other hand, for late IVC, the intake charge decreases when increasing the

363 MVL. These results are in agreement with those find by J. Xu et al. [29] in case of early
364 IVC, and Clenci et al. [37] in case of late IVC.

365 The backflow mass is the difference between the maximum in-cylinder mass during the
366 intake stroke and the in-cylinder mass after the intake valve close. According to Fig. 7
367 (b), the backflow mass decreases almost in all cases with increasing the engine speed for
368 all valve lift law, and it decreases with decreasing the MVL. This can be attributed to the
369 fact that the airflow inertia increases with increasing engine speed which can justify the
370 decrease of backflow mass with engine speed. The effect of IVC on the backflow mass is
371 more significant than the effect of MVL. It can be noted that the backflow mass is
372 significant at ICV70, and very low (insignificant) at IVC30. This is because late IVC
373 could help to expel a portion of in-cylinder charge in the intake port.

374 The aspiration work is a representative of pumping losses; it was calculated through the
375 integral of the in-cylinder pressure from IVO to IVC. Fig. 7 (c) shows the effect of MVL
376 and IVC on the aspiration work for different engine speeds. As seen in Fig. 7 (c),
377 regardless of the IVC, decreasing MVL increases the aspiration work. This can be
378 explained by the fact that lowering MVL decreases the effective flow area. Moreover,
379 increasing engine speed also increases the pumping losses. Similar results were found by
380 J. Xu et al [29].

Fig. 7 (d) shows the effect of IVC and MVL on the maximum pressure (at TDC in case of cold airflow) for various engine speeds. In almost all cases, at Early IVC (IVC30), the in-cylinder peak pressure decreases with speed, except for MVL10.6. However, for all MVL, the in-cylinder peak pressure increases slightly with the speed at IVC50, while it increases considerably at Late IVC (IVC70). Therefore, we can consider that, for most cases, Early IVC increases the in-cylinder peak pressure, and Late IVC decreases the in-cylinder peak pressure. This is in concordance with the results of Jia et al [27] and Zhang et al [28]. Moreover, for Early IVC, the in-cylinder peak pressure increases with increasing MVL, in particular at high speeds, which is in agreement with Clenci et al [37] findings. Our results show that adjusting the IVC and varying the MVL can be a way to control the effective compression ratio. Consequently, as the valve lift law changes, it is recommended to adjust the diesel start of injection, to obtain a better thermal efficiency and thus lower fuel consumption, lower pressure rise rate and reduced exhaust emissions [27]. Indeed, according to Jia et al [27], the ignition timing is controlled by IVC timing, the reduced ignition delay result in advancing the start of combustion, which increases the pressure rise rate and NOx emissions.

Based on previous results, the MVL10 IVC30 (MVL = 10.60 mm and IVC30 °CA ABDC) valve lift law prevents the engine from backfire (backflow very low), allows high volumetric efficiency, high maximum pressure and low pumping losses. Therefore, for the upcoming study, the valve lift law with MVL10 IVC30 is chosen.

To confirm if the valve lift law MVL10 IVC30 chosen with 2D simulations in case of cold airflow, was also valid for the 3D simulations at engine run conditions chosen for this study which are fixed to 90% load, 1500 rpm and 42.5% hydrogen energy share. The existing and recommended valve lift law (IVC70 and IVC30) with Maximum Valve Lift=10.60 mm was used to simulate the cylinder mass and backflow mass with 3D approach for various engine speed, then the results were compared with the 2D simulations ones. Fig. 8 shows the profile of in-cylinder mass and backflow mass for the valve lift law MVL10 IVC70 and MVL10 IVC30 at 90% of load and 42.5% hydrogen energy share using 3D simulation. According to Fig. 8, the 3D results confirm the 2D ones, except for engine speed greater than 2000 rpm. Indeed, unlike the 2D simulations, in 3D ones, the in-cylinder mass is greater in case of IVC70 compared to IVC30 for the engine speed greater than 2000 rpm. However, the backflow mass is very low in case of IV30 for all the engine speed range. This has no effect on the choice of valve lift for this study. This is because, except for engine speed higher than 2000 rpm, the IVC30 case ensures a greater intake charge and there is negligible backflow mass, which prevent the engine from backfiring. Therefore, it can be concluded that 3D simulations confirm the 2D approach at speeds lower than 2000 rpm. In fact, as it was noted by Xu et al [29], the volumetric efficiency increases with the late IVC at high engine speed. On the other hand, it increases with the Early IVC at low engine speed. Our results for 3D simulation are in good agreement with those findings.

3. 2. Hydrogen injector parameters

The aim of this section is to optimize hydrogen injection parameters such as the injection pressure, injector inclination and start of injection. The engine operation conditions were fixed to 90% load, 1500 rpm with hydrogen energy share of 42.5%.

3. 2. 1. Hydrogen injection pressure

To select the hydrogen injection pressure, six hydrogen injection pressures (1.2, 1.7, 2.2, 2.7, 3.7 and 4.5 bar) were examined for the existing and recommended valve lift law and two hydrogen start of injection, therefore, the cases IVC70 HSOI60, IVC30-HSOI60 and IVC30-HSOI43 were considered. To achieve this goal, the hydrogen mass fraction distribution in the air before the intake valve closing was quantified to identify the risk of the flammability of hydrogen in the air, and thus the risk of backfiring for each case.

The injector characteristics curve shown in Fig. 9 is used to determine the hydrogen mass flow and the injection duration corresponding to the provided hydrogen injection pressure.

Fig. 10 shows the profiles of the average hydrogen mass fraction in the intake manifold volume for the valve lift law IVC70-HSOI60, IVC30-HSOI43 and IVC30-HSOI60. In the case IVC70-HSOI60, hydrogen-air mixture is repressed to the intake port for all hydrogen injection pressures before the intake valve closing as seen in Fig. 10 (a). This

means that the mass fraction of hydrogen after intake valve closing is significant and thus, the risk of backfiring is high.

For IVC30, it can be seen from Fig. 10 (b) and (c) that for hydrogen injection pressure of 1.2 bar at both HSOI43 and HSOI60 and hydrogen injection pressure of 1.7 bar at HSOI60, high hydrogen fractions were accumulated in the intake manifold at the intake valve closing. This can be attributed to the high injection duration and the low mass flow rate (see Fig. 9). Which means that, after hydrogen injection ends, the time available for hydrogen to reach the combustion chamber is smaller than the required time [17]. As a result, hydrogen injection pressure of 1.7 bar for HSOI43 and 1.2 bar for both HSOI43 and HSOI60 cannot be used due to the high risk of backfiring.

In the case IVC30-HSOI43, the hydrogen mass fraction is almost zero at the intake manifold after intake valve closing for hydrogen injection pressure of 2.2, 2.7, 3.7 and 4.5 bar, except for hydrogen injection pressure of 1.7 bar, which means that the hydrogen does not completely reach the combustion chamber. In the case IVC30-HSOI60, the hydrogen mass fraction is also almost zero in intake manifold for the hydrogen injection pressure of 2.7, 3.7 and 4.5 bar, but it is not the case for hydrogen injection pressure of 2.2 bar. For those two cases, the hydrogen fraction is too low; therefore, the occurrence of pre-ignition cannot be verified. Consequently, various engine speeds were examined to verify the backfiring risk at these cases.

458 Fig. 11 shows the distributions of hydrogen mass fraction for different engine speeds at
459 hydrogen injection pressure of 1.7 bar in case IVC30-HSOI43, and 2.2 bar in case
460 IVC30-HSOI60 at intake valve closing. The low flammability limit is $\varphi = 0.1$ (fuel-air
461 equivalence ratio) [7], which corresponds to 0.3% mass fraction in hydrogen-air mixture.
462 According to Fig. 11, in the case HSOI43 with P = 1.7 bar, there is a little accumulation
463 of hydrogen in intake port and the fraction reaches the flammability limit only in specific
464 zones at 1000, 1500 and 2500 rpm. In the case HSOI60 with P = 2.2 bar, the
465 accumulation of hydrogen in intake port is significant and the fraction reaches the
466 flammability limit therefore the risk of backfire is greater.

467 As a result, for a fixed injection position and induced hydrogen mass per cycle, the
468 possible hydrogen injection pressures to be used without having the accumulation of
469 hydrogen in intake port and thus the backfiring risk are: 2.2, 2.7, 3.7 and 4.5 bar for
470 IVC30 HSOI43 °CA ATDC and 2.7, 3.7 and 4.5 bar for IVC30-HSOI60 °CA ATDC.

471 **3. 2. 2. Hydrogen start of injection (HSOI)**

472 Fig. 12 shows the profiles of the average in-cylinder temperature as function of the
473 hydrogen injection pressure at 90% load and 1500 rpm for two hydrogen start of injection
474 (HSOI43 and HSOI60 °CA ATDC) and a fixed total injected hydrogen mass (42.5%
475 energy share). Two hydrogen mass fractions have been considered for this study. The
476 first one is 0.001% represented in Fig. 12 (a) which shows that the hydrogen begin

reaching the combustion chamber. The second value is 0.3% (Fig. 12 (b)) which corresponds to the lower flammability limit of the hydrogen-air mixture. Fig. 12 (c) is an example (HSOI43 and 2.7 bar hydrogen injection pressure) which explains how the in-cylinder temperature corresponding to a given in-cylinder hydrogen mass fraction during the intake stroke, is determined. Each point in fig. 12 (a) and (b) is obtained basing on a figure similar to Fig. 12 (c). According to Fig. 12 (a) and (b), the in-cylinder temperature increases with increasing hydrogen injection pressure. This is because hydrogen velocity increases proportionally to the injection pressure which reduces the time taken to reach the combustion chamber. Moreover, the in-cylinder temperature for a constant hydrogen mass fraction is higher at HSOI43 compared to HSOI60. Therefore, HSOI60 is more able to provide a pre-cooling effect and thus, decrease the chance of pre-ignition sources presence and helps to quench any hot residual combustion products. This leads to prevent the engine from backfire and pre-ignition risk [6,8,14]. Thus, for the remaining study, the HSOI60 was chosen.

3. 2. 3. Effect of hydrogen injection pressure and hydrogen injector inclination on mixture quality

A heterogeneous mixture can contribute to deteriorate the engine performance [10,17], and increasing pollutant emissions. It can also increase the risk of pre-ignition and knock. In this section, mixture quality is examined when varying hydrogen injection pressure

and hydrogen injector inclination. Fig. 13 shows the hydrogen mass fraction distribution for two hydrogen injector inclinations (45° and 60°) combined with three hydrogen injection pressures (2.7, 3.7 and 4.5 bar), at a constant engine speed of 1500 rpm and various crank angle positions.

As already seen in Fig. 10 (b), hydrogen injection ends at 175.6, 152.7 and 143.2 °CA ATDC for hydrogen injection pressure of 2.7, 3.7 and 4.5 bar, respectively. The hydrogen injection finished early before IVC for hydrogen injection pressure of 3.7 and 4.5. This means that a considerable amount of air was introduced in intake manifold without mixing with hydrogen (see Fig. 13 (a)). This is explained by the fact that increasing hydrogen injection pressure, increases mass flow rate and thus decreases the injection duration, as already seen in Fig. 9. When the injection pressure is greater than 2.7 bar (3.7 and 4.5 bar), the time available for hydrogen to reach the combustion chamber is more significant compared to the time taken after the end of hydrogen injection. On the other hand, according to Fig. 13 (b), during the end of compression stroke, 150 and 165 °CA ABDC, the hydrogen concentrations are high at the exhaust valve sideway and low at the intake valve sideway for injection pressures 3.7 and 4.5 bar. In addition, the hydrogen injection pressure 2.7 bar was able to enhance the hydrogen-air mixture quality compared to the other tested pressures. This is clearly visible at the 150 and 165 ° CA ABDC as shown in Fig. 13 (b).

The inclination of 60° gives a better mixing quality of hydrogen-air mixture compared to that of 45°. This was observed at the compression stroke (Fig. 13 (b)), where the concentration of hydrogen is higher at exhaust valve sideway and lower at intake valve sideway for hydrogen injector inclination of 45°.

As results, the hydrogen injection pressure 2.7 bar and the injector inclination of 60° allow a good homogeneity of hydrogen-air mixture.

3. 3. Engine Performance

Fig. 14 shows the engine combustion performances, such as in-cylinder pressure and temperature, heat release rate, rate of pressure rise and the exhaust emissions of NOx and CO_2 of the standard diesel mode (D IVC70), and the optimized hydrogen-diesel dual fuel mode (DF IVC30) for hydrogen injection pressure p=2.7 (bar), at an engine speed of 1500 rpm.

An increase of peak in-cylinder pressure, rate of pressure rise, in-cylinder temperature and heat release rate with dual fuel mode, is observed from Fig. 14. This is due to the higher burning velocity and diffusivity of hydrogen [2,13] that speeds up the initiation of the premixed combustion and help to achieve the complete and almost instantaneous combustion of the air-fuel mixture.

Moreover, the concentration of CO_2 emissions is lower in hydrogen-diesel dual fuel engine compared to conventional diesel engine. This is due to the use of hydrogen which

534 is a free carbon fuel, and the improvement of the combustion efficiency with hydrogen
535 addition.

536 However, the NO_x specific emissions were higher with hydrogen-diesel dual fuel mode
537 compared to the conventional diesel engine in these operating conditions. The increase of
538 these emissions is mainly due to the rise of in-cylinder temperature [2,15] and high
539 residence time of the high temperature gases in the cylinder [43].

540 **3. 4. Effect of diesel SOI**

541 While investigating the hydrogen-diesel dual fuel engine combustion characteristics, it is
542 crucial to investigate the diesel start of injection (DSOI) timing. Therefore, Fig. 15 shows
543 the effect of retarding DSOI by 0, 3, 5, 8, 10 and 12 °CA compared to baseline case, on
544 combustion characteristics and exhaust emissions of NO_x and CO_2. It can be observed
545 from Fig. 15 that retarding DSOI to values higher than 8 °CA, decreases the peak in-
546 cylinder pressure, in-cylinder temperature and the rate of pressure rise. However, it has
547 not a great effect on the rate of heat release (HRR). A decrease of CO_2 emissions with
548 increasing DSOI delay was also observed. Furthermore, according to Fig. 15, NO_x
549 specific emissions decreased while retarding DSOI to values higher than 8 °CA. This is
550 because decreasing the in-cylinder temperature helps to reduce thermal NO_x formation.

551

4. Conclusion

Numerical 2D and 3D dynamic simulations using CFD code ANSYS Fluent was performed for a single cylinder hydrogen-diesel dual fuel engine. An attempt to optimize the hydrogen TMI system through valve lift law (maximum valve lift and IVC timing) and hydrogen injection parameters (pressure, inclination and injection timing) was performed, in order to prevent the backfire phenomena, improve the volumetric efficiency and the mixture formation quality of a hydrogen-diesel dual-fuel engine. The following results were obtained:

1. The valve lift law MVL10.6 IVC30 (MVL=10.60 (mm) and IVC=30 (°CA ABDC)) is the optimum choice because it reduces the risk of backfire and pre-ignition while ensuring a high volumetric efficiency.

2. The HSOI60 (°CA ATDC) is able to provide a pre-cooling effect and thus, could reduce the pre-ignition sources and helps to quench any hot residual combustion product.

3. The hydrogen injection pressure of 2.7 (bar) and an inclination of 60° helps to improve the quality of hydrogen-air mixture.

4. The optimized hydrogen-diesel dual fuel mode shows an increase of the peak in-cylinder pressure, in-cylinder temperature, heat release rate, rate of pressure rise,

and NOx specific emissions comparing to the diesel engine. However, a decrease of the concentration of CO_2 emissions was observed for the dual fuel mode.

5. For values of DSOI retard higher than 8 (°CA), the peak in-cylinder pressure, in-cylinder temperature, the rate of pressure rise and NOx emissions are similar or lower for hydrogen-diesel dual fuel engine compared with diesel engine.

Nomenclature

ABDC	After Bottom Dead Center
ATDC	After Top Dead Center
BDC	Bottom Dead Center
BTDC	Before Top Dead Center
CA	Crank Angle
CFD	Computational Fluid Dynamics
CMI	Continuous Manifold Injection
CNG	Compressed Natural Gas
CO	Carbon Monoxide (%)
CO2	Carbon Dioxide (%)
D	Diesel engine
DF	Dual Fuel engine
DSOI	Diesel Start Of Injection (°CA)
EMIV	Electromagnetic Intake Valve Train
HC	Unburned Hydrocarbon

592	HSOI	Hydrogen Start Of Injection (°CA)
593	HSOI43	Hydrogen Start Of Injection at 43 (°CA)
594	HSOI60	Hydrogen Start Of Injection at 60 (°CA)
595	HRR	Heat Release Rate (J/ °CA)
596	IVC	Inlet Valve Closing (°CA)
597	IVC30	Intake valve is closed at 30 °CA ABDC
598	IVC50	Intake valve is closed at 50 °CA ABDC
599	IVC70	Intake valve is closed at 70 °CA ABDC
600	IVO	Intake Valve Open (°CA)
601	MVL	Maximum Valve Lift (mm)
602	NOx	oxides of nitrogen (ppm)
603	Rpm	Rotation per minutes
604	TDC	Top Dead Center
605	TMI	Timed Manifold Injection
606	SOI	Start Of Injection (°CA)
607	UDF	User Defined Function

608	YH2, YCO2,	mass fraction of H_2 (%), CO_2 (%) respectively
609	YNOx	mass fraction of NOx (ppm)
610	θ	Crank Angle Degree (°CA)

Acknowledgments

This research was supported by the Algerian General Directorate for Scientific Research and Technological Development (DG-RSDT) and Renewable Energy Development Center. Research project with socio-economic impact (PISE/HYD/01).

615 **References**

616 [1] H. Köse, M. Ciniviz. An experimental investigation of effect on diesel engine
617 performance and exhaust emissions of addition at dual fuel mode of hydrogen. Fuel
618 Processing Technology 2013; 114: 26–34.

619 [2] Deb M, Sastry GRK, Bose PK, Banerjee R. An experimental study on combustion,
620 performance and emission analysis of a single cylinder, 4-stroke DI-diesel engine using
621 hydrogen in dual fuel mode of operation. Int J Hydrogen Energy 2015; 40:8586–98.

622 [3] Saravanan N, Nagarajan G, Sanjay G, Dhanasekaran C, Kalaiselvan KM. Combustion
623 analysis on a DI diesel engine with hydrogen in dual fuel mode. Fuel 2008; 87:3591–9.

624 [4] Saravanan N, Nagarajan G. An insight on hydrogen fuel injection techniques with
625 SCR system for NOx reduction in a hydrogen–diesel dual fuel engine. Int J Hydrogen
626 Energy 2009; 34:9019–32.

627 [5] Deb M, Paul A, Debroy D, Sastry GRK, Panua RS, Bose PK. An experimental
628 investigation of performance-emission trade off characteristics of a CI engine using
629 hydrogen as dual fuel. Energy 2015; 85:569–85.

630 [6] Liu X, Liu F, Zhou L, Sun B, Schock HJ. Backfire prediction in a manifold injection
631 hydrogen internal combustion engine. Int J Hydrogen Energy 2008; 33:3847–55.

632

633 [7] Verhelst S, Wallner T. Hydrogen-fueled internal combustion engines. Prog Energy
634 Combust Sci 2009; 35:490–527.

635 [8] Lee KJ, Huynh TC, Lee JT. A study on realization of high performance without
636 backfire in a hydrogen-fueled engine with external mixture. Int J Hydrogen Energy 2010;
637 35: 13078–87.

638 [9] Lee JT, Lee KJ, Jonggoo L, Byunghoh A. High power performance with zero NOx
639 emission in a hydrogen-fueled spark ignition engine by valve timing and lean boosting.
640 Fuel 2014; 128: 381–9.

641 [10] DAS L.M. Fuel induction techniques for a hydrogen operated engine. Int J Hydrogen
642 Energy 1990; 15: 833–42.

643 [11] White CM, Steeper RR, Lutz AE. The hydrogen-fueled internal combustion engine:
644 a technical review. Int J Hydrogen Energy 2006; 31:1292–305.

645 [12] Das L.M. Hydrogen engine: research and development (R&D) programs in Indian
646 Institute of Technology (IIT), Delhi. Int J Hydrogen Energy 2002; 27: 953–65.

647 [13] Tarkan S, Yasin K. Experimental investigation of the combustion characteristics,
648 emissions and performance of hydrogen port fuel injection in a diesel engine. Int J
649 Hydrogen Energy 2014; 39: 18480–89.

650 [14] Deb M, Majumder A, Banerjee R, Sastry GRK, Bose PK. A Taguchi-fuzzy based
651 multi-objective optimization study on the soot-NOx-BTHE characteristics of an existing
652 CI engine under dual fuel operation with hydrogen. Int J Hydrogen Energy 2014; 39:
653 20276–93.

654 [15] Chintala V, Subramanian KA. Experimental investigation of hydrogen energy share
655 improvement in a compression ignition engine using water injection and compression
656 ratio. Energy Convers Manage 2016; 108:106–19.

657 [16] Wang L, Yang Z, Huang Y, Liu D, Duan J, Guo S, Qin Z. The effect of hydrogen
658 injection parameters on the quality of hydrogen-air mixture formation for a PFI hydrogen
659 internal combustion engine. Int J Hydrogen Energy 2017; 42: 23832–45.

660 [17] Chintala V, Subramanian KA. A CFD (computational fluid dynamics) study for
661 optimization of gas injector orientation for performance improvement of a dual-fuel
662 diesel engine. Energy2013; 57: 709–21.

663 [18] Cheng X, Baigang S, Zhen H. Investigation on jet characteristics of hydrogen
664 injection and injection strategy for backfire control in a port fuel injection hydrogen
665 engine. Energy Procedia 2017; 105: 1588–99.

[19] Yang B, Xi C, Wei X, Zeng K, Lai M. Parametric investigation of natural gas port injection and diesel pilot injection on the combustion and emissions of a turbocharged common rail dual-fuel engine at low load. Appl Energy 2015; 143: 130–7.

[20] Saravanan N, Nagarajan G, Dhanasekaran C, Kalaiselvan KM. Experimental investigation of hydrogen port fuel injection in DI diesel engine. Int J Hydrogen Energy 2007; 32: 4071–80.

[21] Yang Z, Zhang F, Wang L, Wang K, Zhang D. Effects of injection mode on the mixture formation and combustion performance of the hydrogen internal combustion engine. Energy 2018; 147: 715-28.

[22] Chintala V, Subramanian K.A. experimental investigation of autoignition of hydrogen-air charge in a compression ignition engine under dual-fuel mode. Energy 2017; 138: 197-209.

[23] Salvi B.L, Subramanian K.A. Experimental investigation on effects of compression ratio and exhaust gas recirculation on backfire, performance and emission characteristics in a hydrogen fuelled spark ignition engine. . Int J Hydrogen Energy 2016; 41: 5842-55.

[24] Tsujimura T, Suzuki Y. Development of a large-sized direct injection hydrogen engine for a stationary power generator. Int J Hydrogen Energy (2018). doi.org/10.1016/j.ijhydene.2018.09.178.

[25] Dhyani V, Subramanian K.A. Experimental investigation on effects of knocking on backfire and its control in a hydrogen fueled spark ignition engine. Int J Hydrogen Energy 2018; 43: 7169-78.

[26] Dhyani V, Subramanian K.A. Control of backfire and NOx emission reduction in a hydrogen fueled multi-cylinder spark ignition engine using cooled EGR and water injection strategies. Int J Hydrogen Energy. https://doi.org/10.1016/j.ijhydene.2019.01.129.

[27] Jia M, Xie M, Wang T, Peng Z. The effect of injection timing and intake valve close timing on performance and emissions of diesel PCCI engine with a full engine cycle CFD simulation. Appl Energy 2011; 88: 2967–75.

[28] Zhang X, Wang H, Zheng Z , Reitz RD, Yao M. Effects of late intake valve closing (LIVC) and rebreathing valve strategies on diesel engine performance and emissions at low loads. Appl Therm Eng 2016; 98: 310–9.

[29] Xu J, Chang S, Fan X, Fan A. Effects of electromagnetic intake valve train on gasoline engine intake charging. Appl Therm Eng 2016; 96: 708-15.

[30] Li N, Xie H, Chen T, Li L, Zhao H. The effects of intake backflow on in-cylinder situation and auto ignition in a gasoline controlled auto ignition engine. Appl Energy 2013; 101: 756–64.

[31] Cinar C, Uyumaz A, Solmaz H, Topgul T. Effects of valve lift on the combustion and emissions of a HCCI gasoline engine. Energy Convers Manage 2015; 94: 159–68.

[32] Verhelst S, Demuynck J, Sierens R, Huyskens P. Impact of variable valve timing on power, emissions and backfire of a bi-fuel hydrogen/gasoline engine. Int J Hydrogen Energy 2010; 35, 4399–4408.

[33] Awad S, Contribution à l'étude de la valorisation énergétique des résidus graisseux et de leur combustion dans les moteurs à combustion interne. Université de Nantes 2011: Thèse de Doctorat.

[34] Bari S, Saad I. CFD modelling of the effect of guide vane swirl and tumble device to generate better in-cylinder air flow in a CI engine fuelled by biodiesel. Computers & Fluids 2013; 84: 262–9.

[35] Shojaeefard MH, Noorpoor AR. Flow Simulation in Engine Cylinder with Spring Mesh. American Journal of Applied Sciences 2008; 5: 1336–43.

[36] Lakshminarayanan PA, Yogesh VQ. Modelling Diesel Combustion. Springer Netherlands 2010.

[37] Clenci AC, Iorga-Siman V, Deligant M, Podevin P, Descombes G, Niculescu R. A CFD (computational fluid dynamics) study on the effects of operating an engine with low intake valve lift at idle corresponding speed. Energy 2014; 71: 202–17.

720 [38] Merker GP, Schwarz C, Teichmann R. Combustion Engines Development: Mixture
721 Formation, Combustion, Emissions and Simulation, Springer, Berlin, 2012.

722 [39] Abagnale C, Cameretti MC, De Simio L, Gambino M, Iannaccone S, Tuccillo R.
723 Numerical simulation and experimental test of dual fuel operated diesel engines. Appl
724 Therm Eng 2014; 65: 403–17.

725 [40] Cameretti MC, Tuccillo R, De Simio L, Iannaccone S, Ciaravola U. A numerical and
726 experimental study of dual fuel diesel engine for different injection timings. Appl Therm
727 Eng 2016; 101: 630–8.

728 [41] Hairuddin A, Yusaf T, Wandel AP. A review of hydrogen and natural gas addition in
729 diesel HCCI engines. Renew Sust Energy Rev 2014; 32: 739–61.

730 [42] Chintala V, Subramanian K.A. CFD analysis on effect of localized in-cylinder
731 temperature on nitric oxide (NO) emission in a compression ignition engine under
732 hydrogen-diesel dual-fuel mode. Energy 2016; 116:470-488.

733 [43] Deb M, Sastry GRK, Panua RS, Banerjee R, Bose PK. Effect of Hydrogen-Diesel
734 Dual Fuel Combustion on the Performance and Emission Characteristics of a Four
735 Stroke-Single Cylinder Diesel Engine. World Academy of Science, Engineering and
736 Technology International Journal of Mechanical, Aerospace, Industrial, Mechatronic and
737 Manufacturing Engineering 2015; 9: 848-54.

738 **Table captions**

739 Table 1. Engine and diesel fuel injector characteristics

740 Table 2. Gas injector characteristics

741 Table 3. Number of Cells for tested meshes

742

743

744 Table 1. Engine and diesel fuel injector characteristics

Description	Parameter value
type	Lister petter TS1
No. of cylinders	1
Displacement volume (cm^3)	630
Rated output (kw)	4.5 at 1500 rpm
Rated Speed (rpm)	1500
Bore × Stroke (mm)	95.3 × 88.9
Compression ratio	18.0 :1
Connecting rood length (mm)	165.3
Intake valve opening and closing	36 (°CA BTDC) , 69 (°CA ABDC)
Exhaust valve opening and closing	76 (°CA BTDC) and 32 (°CA ABDC)
Diesel start of injection	15 (°CA BTDC)
Injection pressure (bar)	250
Number of holes	4

745

746

747

748 Table 2. Gas injector characteristics

Description	Parameter value
Gas injector	DYMCO Corp/GISM-i1000
Approval Pressure (bar)	1.2 ± 0.1
Operating Temperature Range (°C)	-40 ~ +120
Operating Voltage Range (V)	DC 6~ DC 18
Operating working pressure, relative, (bar)	0.2 to 4.2
Maximum working pressure, relative, (bar)	4.5
Opening time (ms)	3.00
Closing time (ms)	1.00
Injector hole diameter (mm)	1.8

749

Table 3. Number of Cells for tested meshes

		Case1	Case 2	Case 3	Case 4	Case 5	Case 6	Case 7
3D	TDC	305,331	315,831	337,848	380,978	444,665	457,265	474,065
	BDC	810,771	1,057,271	1,072,888	1,114,578	1,180,745	1,421,805	1,908,305
2D	TDC	4,636	5,028	6,146	6,709	12,258	12,694	17,472
	BDC	15,667	18,646	23,946	32,929	38,490	47,602	82,880

Figure captions

Fig. 1. Inlet and exhaust duct geometry with gas injector position

Fig. 2. 2D and 3D mesh at (a) TDC, (b) BDC with geometry decomposition

Fig. 3. Intake valve profiles

Fig. 4. (a) Grid and (b) time step sensitivity for 2D and 3D mesh

Fig. 5. In-cylinder volume and mass evolution in the 2D and 3D approaches

Fig. 6. Validation of the 2D and 3D simulations

Fig. 7. (a) In-cylinder mass, (b) Backflow mass, (c) Pumping loss work and (d) Maximum pressure for different IVC and MVL under various speeds

Fig. 8. In-cylinder mass and backflow mass under different engine speed

Fig. 9. Characteristics curve of the hydrogen injector

Fig. 10. Hydrogen mass fraction in intake manifold

Fig. 11. Hydrogen mass fraction distribution in case HSOI43 P=1.7 and HSOI60 P=2.2 at various engine speed

Fig. 12. In-cylinder temperature of hydrogen-air mixture at a specific mass fraction of hydrogen

Fig. 13. Hydrogen mass fraction distribution at different pressure injection and inclination for N=1500 rpm, HSOI60 and IVC30

Fig. 14. Combustion characteristics and exhaust emissions of diesel (DF IVC70) and dual fuel (D IVC30)

779 Fig. 15. Effect of retarding the diesel start of injection in combustion characteristics and
780 exhaust emissions

781

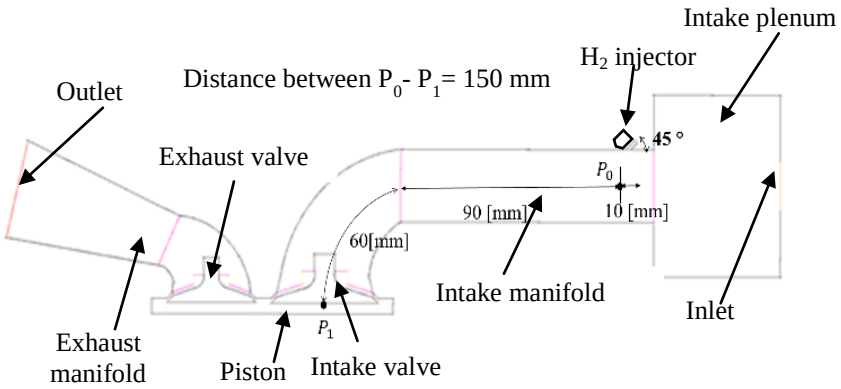

Fig. 1. Inlet and exhaust duct geometry with gas injector position

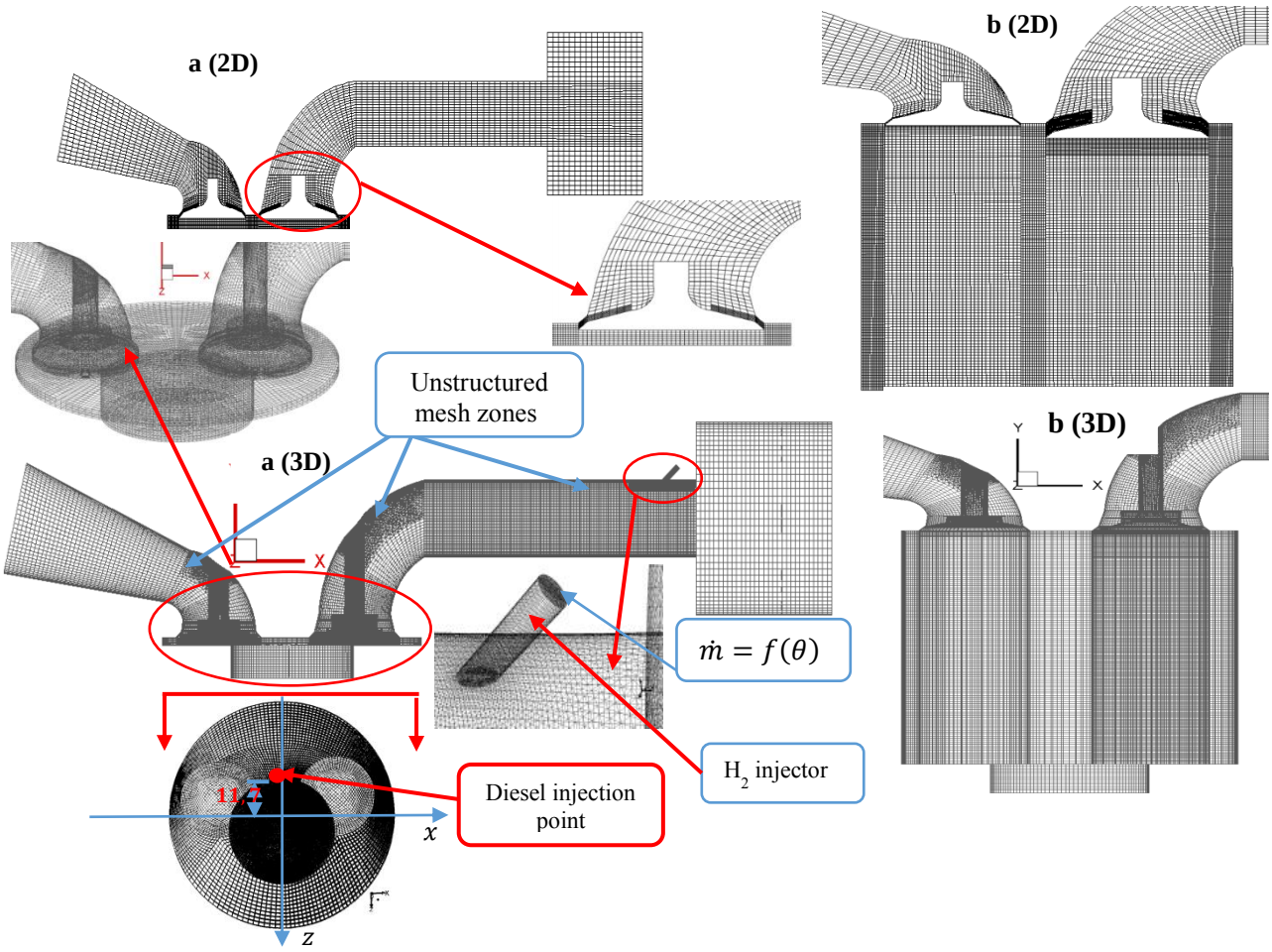

Fig. 2. 2D and 3D mesh at (a) TDC, (b) BDC with geometry decomposition

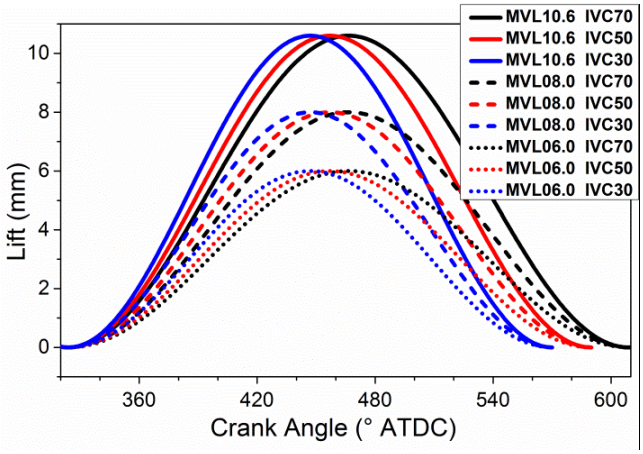

Fig. 3. Intake valve profile

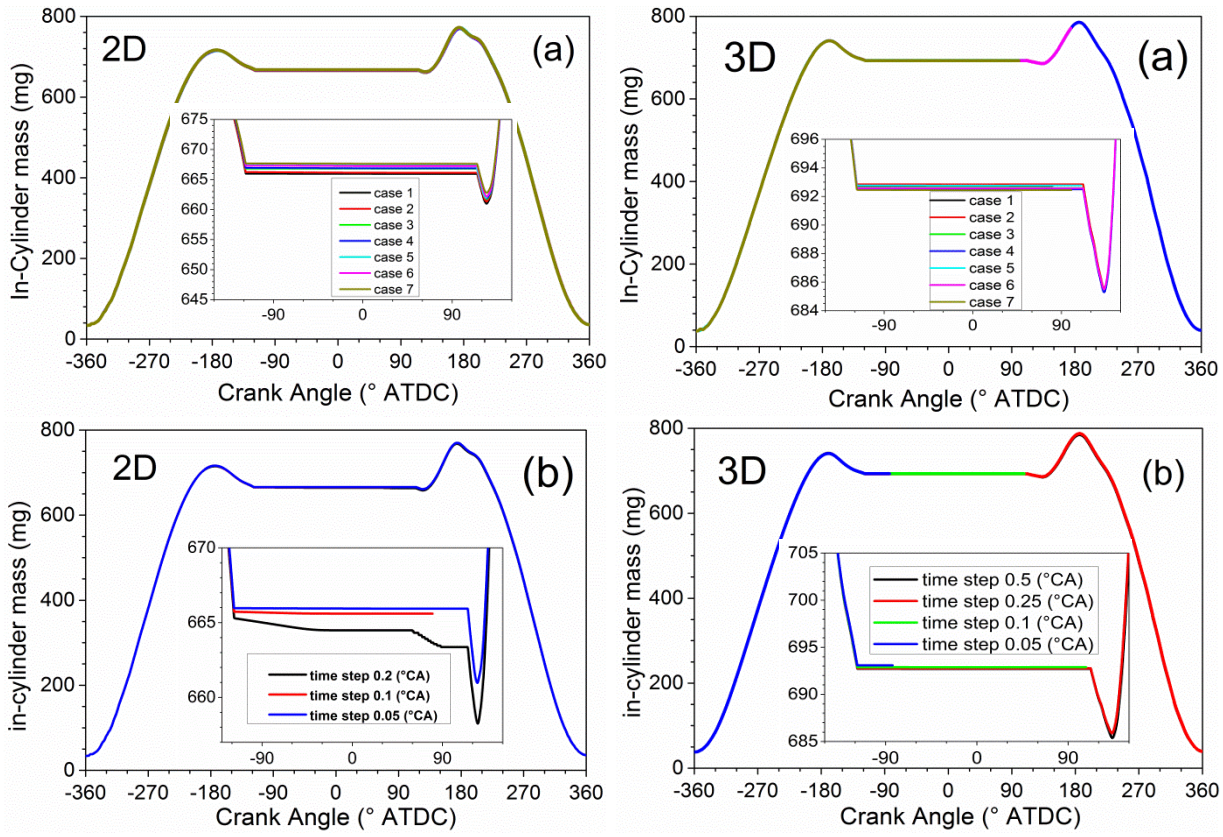

Fig. 4. (a) Grid and (b) time step sensitivity for 2D and 3D mesh

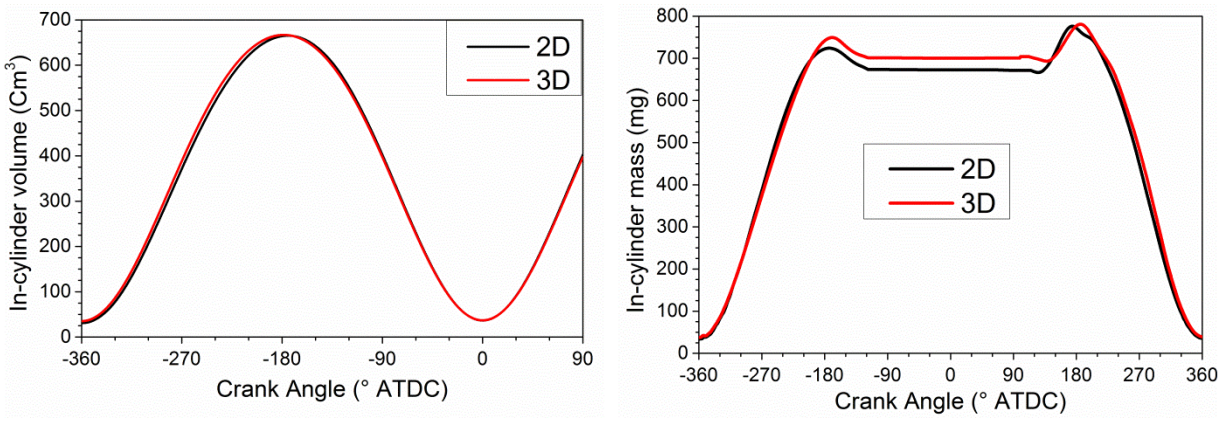

Fig. 5. In-cylinder volume and mass evolution in the 2D and 3D approaches

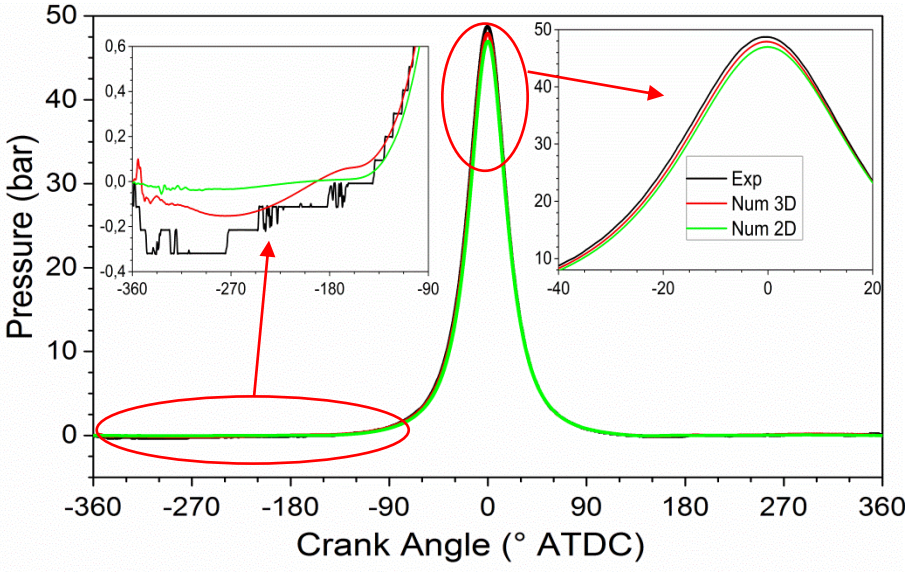

Fig. 6. Validation of the 2D and 3D simulations

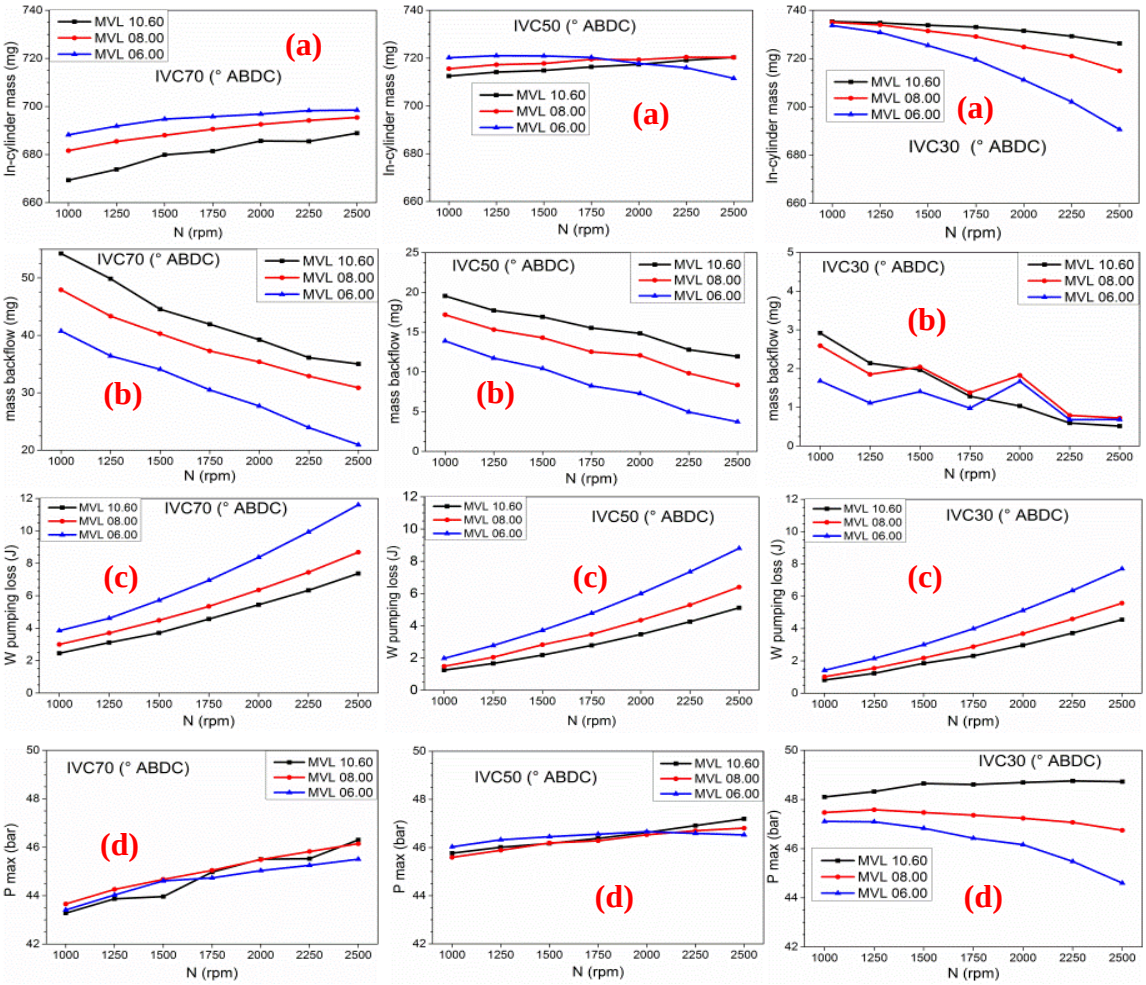

Fig. 7. (a) In-cylinder mass, (b) Backflow mass, (c) Pumping loss work and (d) Maximum pressure for different IVC and MVL under various speeds

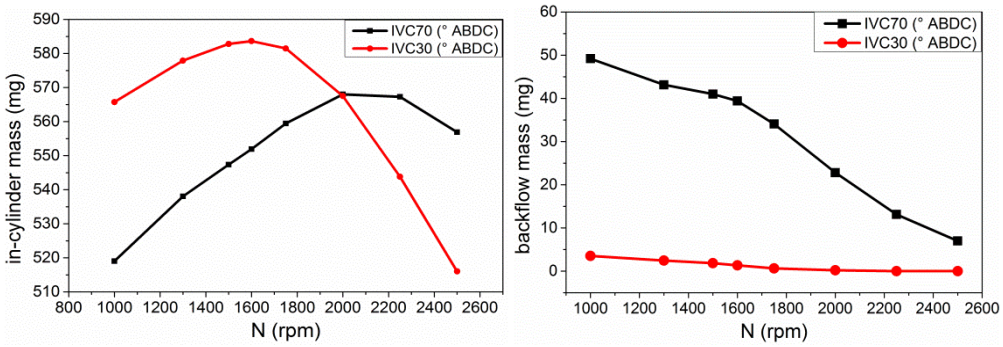

Fig. 8. In-cylinder mass and backflow mass under different engine speed

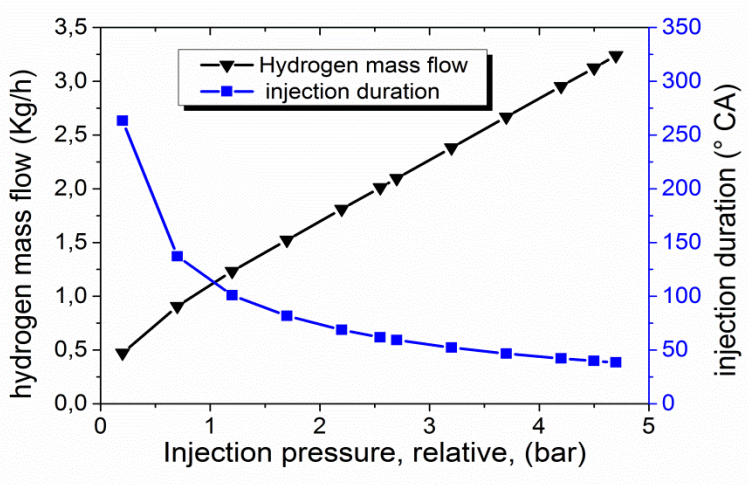

Fig. 9. Characteristics curve of the hydrogen injector

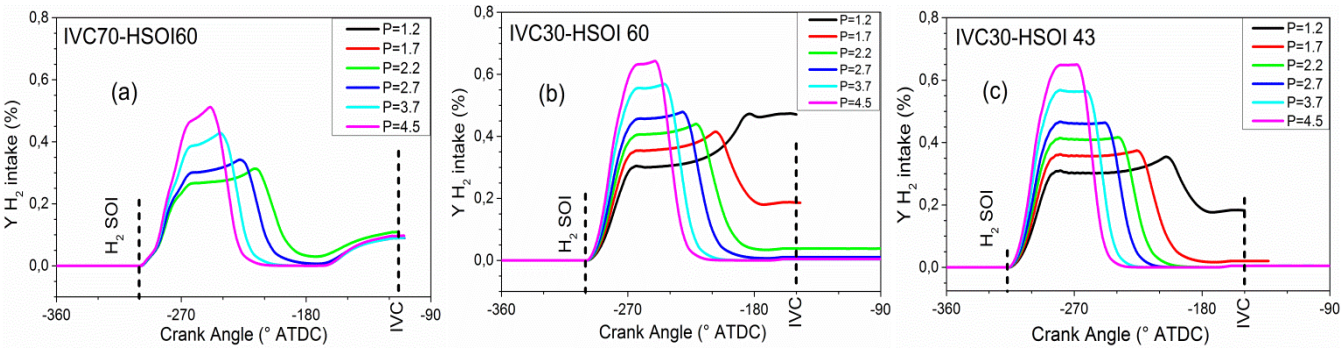

Fig. 10. Hydrogen mass fraction in intake manifold

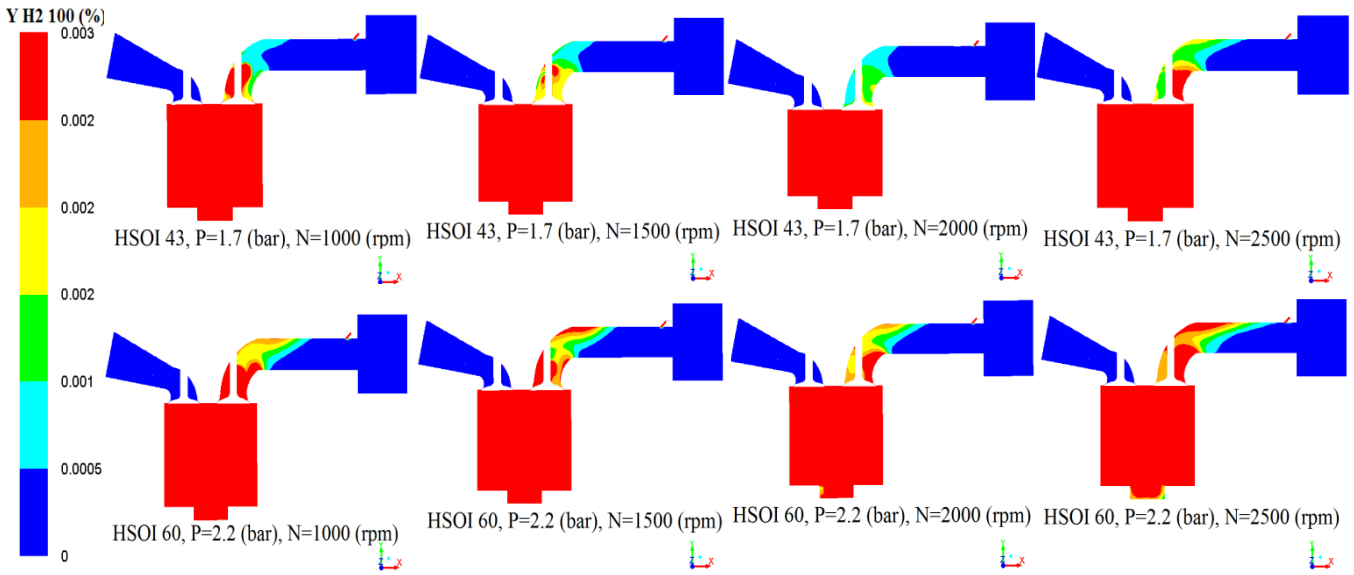

Fig. 11. Hydrogen mass fraction distribution in case HSOI43 P=1.7 and HSOI60 P=2.2 at various engine speed

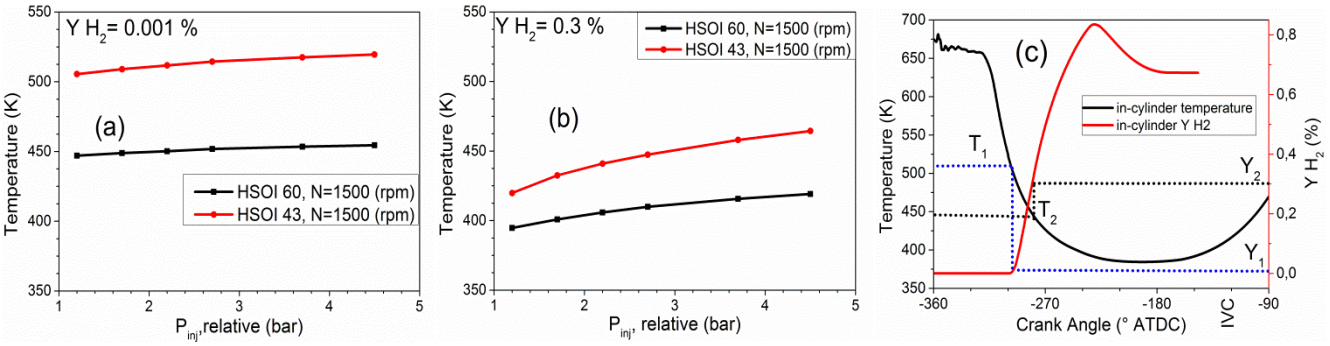

Fig. 12. In-cylinder temperature of hydrogen-air mixture at a specific mass fraction of hydrogen

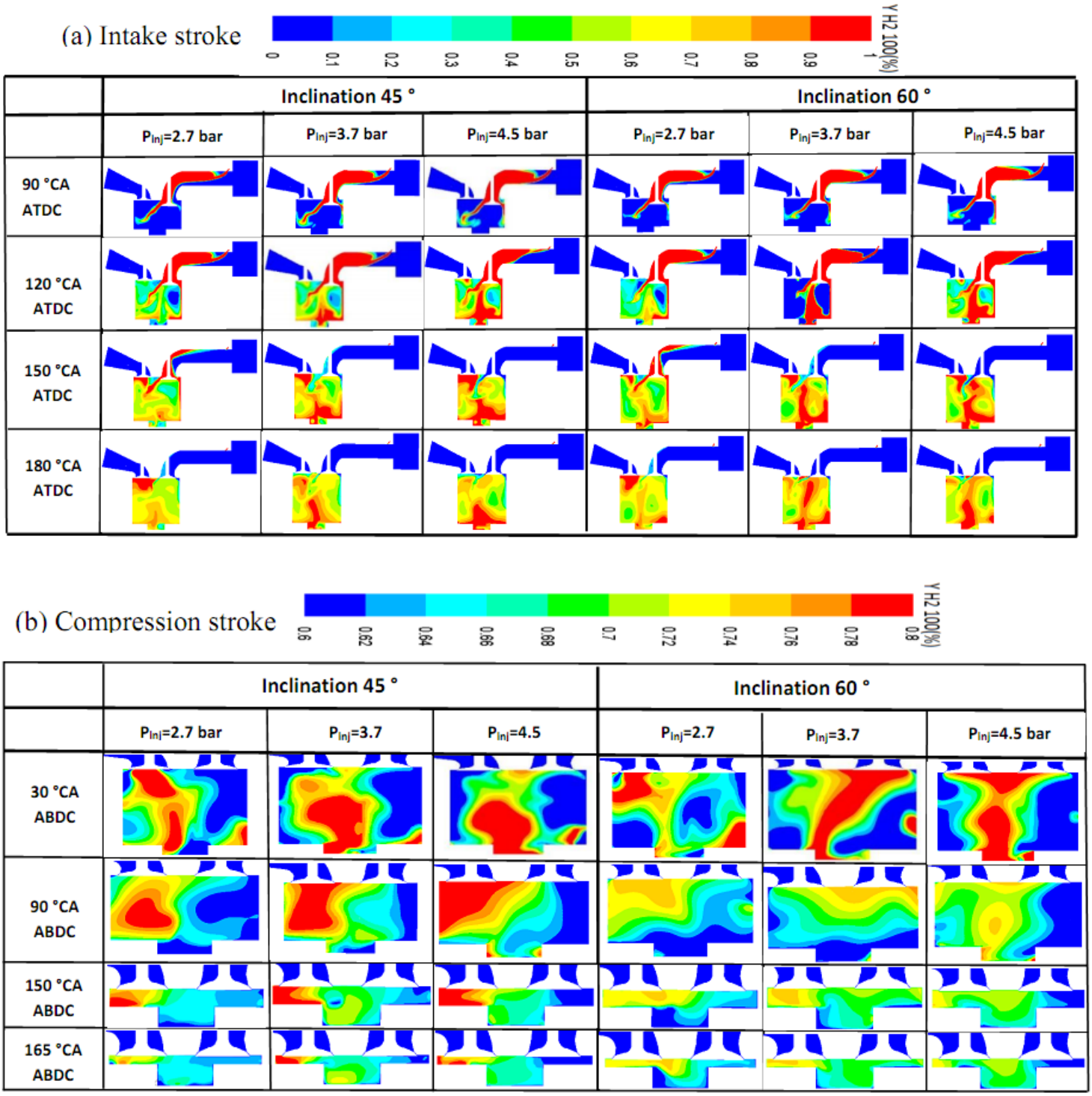

Fig. 13. Hydrogen mass fraction distribution at different pressure injection and inclination for N=1500 rpm, HSOI60 and IVC30

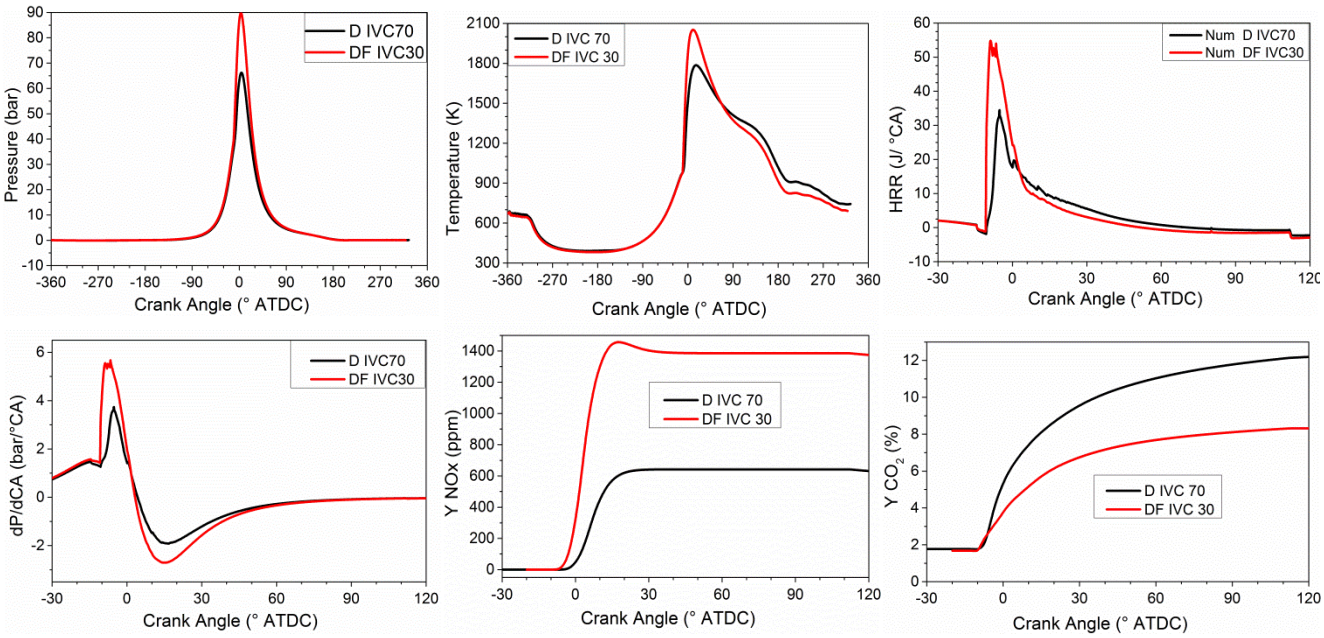

Fig. 14. Combustion characteristics and exhaust emissions of diesel (D IVC70) and dual fuel (DF IVC30)

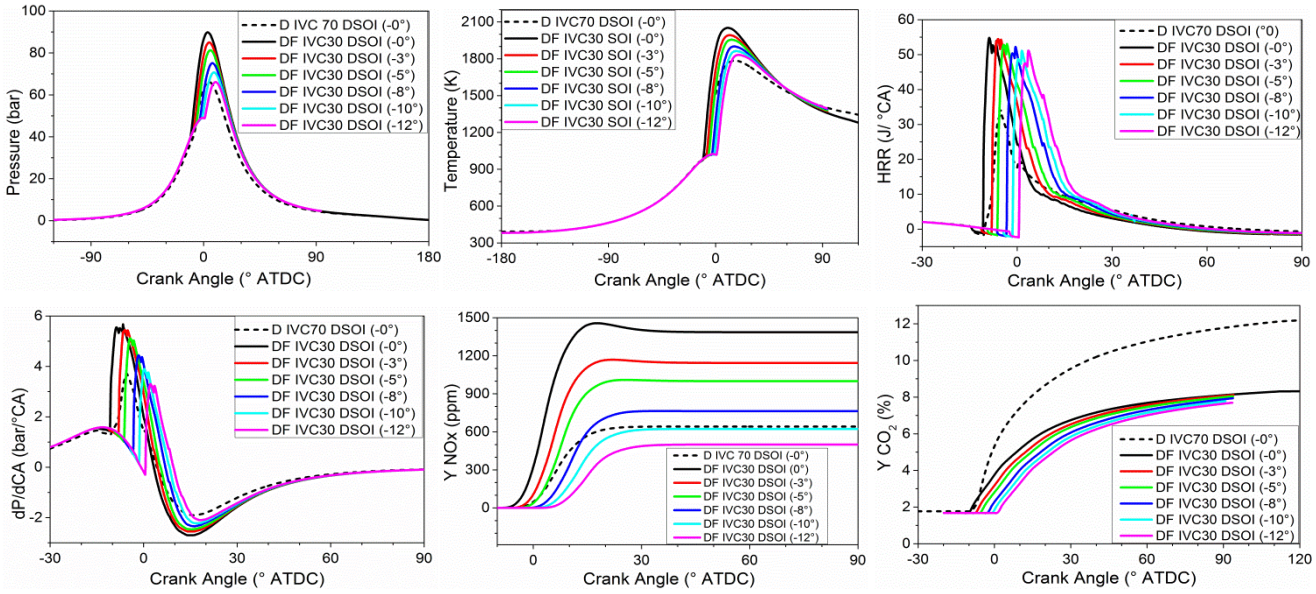

Fig. 15. Effect of retarding the diesel start of injection in combustion characteristics and exhaust emissions